REPORT DOCUMENTATION PAGE

Form Approved OMB No. 0704-0188

1. REPORT DATE *(DD-MM-YYYY)*	2. REPORT TYPE	3. DATES COVERED *(From – To)*
11-01-2010	Final Report	3 September 2008 - 03-Sep-09

4. TITLE AND SUBTITLE

Aeroelastic Scaling of a Joined Wing Aircraft Concept

5a. CONTRACT NUMBER
FA8655-08-1-3071

5b. GRANT NUMBER

5c. PROGRAM ELEMENT NUMBER

6. AUTHOR(S)

Professor Afzal Suleman

5d. PROJECT NUMBER

5d. TASK NUMBER

5e. WORK UNIT NUMBER

7. PERFORMING ORGANIZATION NAME(S) AND ADDRESS(ES)

Instituto Superior Tecnico
Departmento de Engenharia Mecanica
Av. Rovisco Pais, 1
Lisbon 1049-001
Portugal

8. PERFORMING ORGANIZATION REPORT NUMBER

N/A

9. SPONSORING/MONITORING AGENCY NAME(S) AND ADDRESS(ES)

EOARD
Unit 4515 BOX 14
APO AE 09421

10. SPONSOR/MONITOR'S ACRONYM(S)

11. SPONSOR/MONITOR'S REPORT NUMBER(S)
Grant 08-3071

12. DISTRIBUTION/AVAILABILITY STATEMENT

Approved for public release; distribution is unlimited.

13. SUPPLEMENTARY NOTES

14. ABSTRACT

This report is a summary of the work completed within the framework of collaborative research between Instituto Superior Tecnico and the U.S. Air Force (AFRL - WPAFB) under the Grant/Cooperative Agreement Award No. FA8655-05-1-3076. The overall project goal is to produce a 1/9th scale, flight worthy test article for investigating the gust and flutter response of the Boeing Joined-Wing Sensorcraft Concept. While work has continued on the aeroelastic scaling processes, this past years work focuses primarily on the development of an intermediate, rigid flight test vehicle. Construction of the test article took place over the summer in Sintra, Portugal. A newly developed facility in Victoria will soon be operational where building will continue into the New Year. The building of the aircraft is on track for completion in July of 2010 with initial flights to commence at the end of the summer at the Portuguese Air Force Base in Ota. Several issues remain with regards to the stability and controllability of the aircraft and a short flight test windows. Several methods are proposed to address these issues
Finally, an autopilot system was purchased and flown on board a commercially available RC trainer aircraft. The aircraft was flow successfully under automatic control in October of this year. Flight testing is to continue into the new year with the goal of performing a "dry run" of the Rigid Sensorcraft's flight test program in the spring.

15. SUBJECT TERMS
EOARD, Structural Dynamics, Flight testing, Aeroelasticity

16. SECURITY CLASSIFICATION OF:			17. LIMITATION OF ABSTRACT	18, NUMBER OF PAGES	19a. NAME OF RESPONSIBLE PERSON
a. REPORT	b. ABSTRACT	c. THIS PAGE			Surya Surampudi
UNCLAS	UNCLAS	UNCLAS	UL	36	19b. TELEPHONE NUMBER *(Include area code)* +44 (0)1895 616021

EOARD AWARD No. FA8655-08-1-3071

2009 Final Report

Aeroelastic Scaling of a Joined-Wing Aircraft Concept

Principle Investigator | Afzal Suleman

December 2009

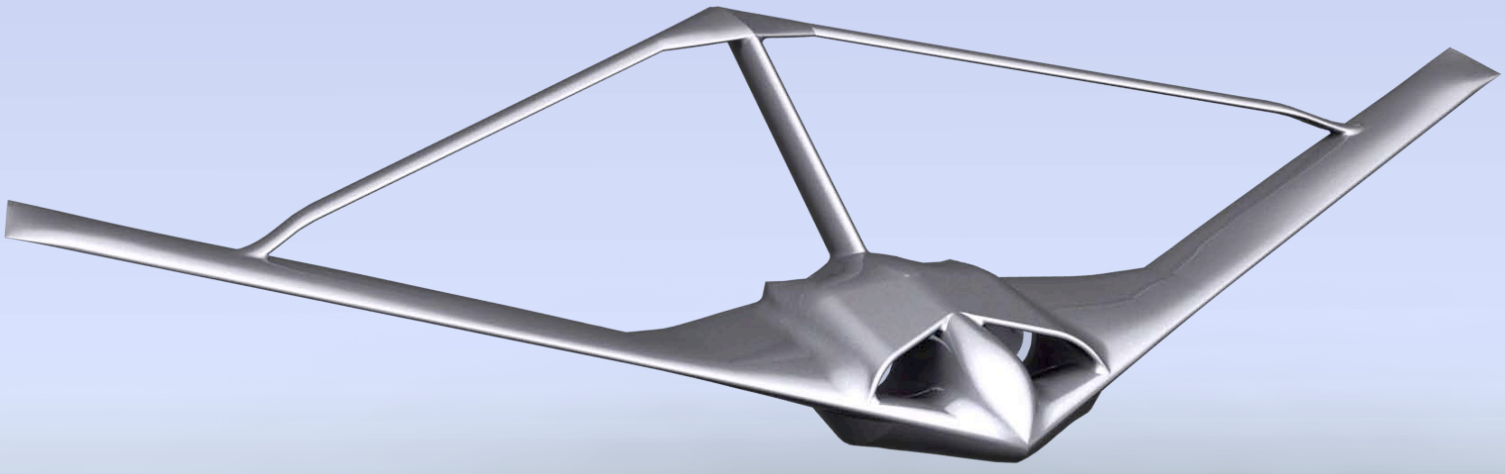

Executive Summary

This report is a summary of the work completed within the framework of collaborative research between Instituto Superior Tecnico and the U.S. Air Force (AFRL - WPAFB) under the Grant/Cooperative Agreement Award No. FA8655-08-1-3071.

The overall project goal is to produce a 1/9th scale, flight worthy test article for investigating the gust and flutter response of the Boeing Joined-Wing Sensorcraft Concept. While work has continued on the aeroelastic scaling processes, this past year's work focuses primarily on the development of an intermediate, rigid flight test vehicle.

Construction of the test article took place over the summer in Sintra, Portugal. A newly developed facility in Victoria will soon be operational where building will continue into the New Year. The building of the aircraft is on track for completion in July of 2010, with initial flights to commence at the end of the summer at the Portuguese Air Force Base in Ota.

Several issues remain with regards to the stability/ controllability of the aircraft and a short flight test window. Several methods are proposed to address these issues but additional information (in the form of aircraft polars and stability derivatives from wind tunnel data and/or higher fidelity studies) would aid greatly in the accuracy and effectiveness of these studies. Any assistance we can receive on this front from either AFIT/ARFL and/or Boeing would be of great help.

Finally, an autopilot system was purchased and flown on-board a commercially available RC trainer aircraft. The aircraft was flown successfully under automatic control in October of this year. Flight testing is to continue into the New Year with the goal of performing a "dry run" of the Rigid Sensorcraft's flight test program in the spring.

Figures

Tables

1 Introduction

The following report serves as a summary of the work completed within the framework of collaborative research between Instituto Superior Tecnico and the U.S. Air Force (AFRL - WPAFB) under the Grant/Cooperative Agreement Award No. FA8655-05-1-3076. The overall project goal is to produce a 1/9th scale, flight worthy test article for investigating the gust and flutter response of the Boeing Joined-Wing Sensorcraft Concept.

As an intermediate step towards this goal, an aerodynamically equivalent, rigid test article will be flown to investigate the flying qualities and flightworthiness of the test platform. This report focuses on several aspects of the design, building and testing of this rigid prototype.

1.1 Overall Project Summary

The overall goal of this group is to develop a flight worthy, reduced scale Remotely Piloted Vehicle (RPV) for use in investigating the linear/non-linear behavior of Boeings Joined Wing concept (410E8). A particular point in the full scale aircraft's flight envelope has been given to investigate which corresponds to a full fuel condition shortly after takeoff.

A reduced scale test point is chosen based on the choice of several parameters, such as overall vehicle size and the altitude at which test flights will take place (chosen to be a 5 meter span with testing to be conducted at 400 meters above sea level). The relationship between the full scale and reduced scale parameters is used to determine a set of derived scaling factors based on a set of governing non-dimensional equations. In the present case, a simplified physics model is chosen; the small disturbance, linear potential partial differential equations (PDE).

$$\begin{bmatrix} \bar{\boldsymbol{M}}_{11} & \bar{\boldsymbol{M}}_{12} \\ \bar{\boldsymbol{M}}_{21} & \bar{\boldsymbol{M}}_{22} \end{bmatrix} \begin{Bmatrix} \ddot{\boldsymbol{\xi}} \\ \ddot{\boldsymbol{\phi}} \end{Bmatrix} + \begin{bmatrix} \bar{\boldsymbol{K}}_{11} & \bar{\boldsymbol{K}}_{12} \\ \bar{\boldsymbol{K}}_{21} & \bar{\boldsymbol{K}}_{22} \end{bmatrix} \begin{Bmatrix} \boldsymbol{\xi} \\ \boldsymbol{\phi} \end{Bmatrix} = \begin{bmatrix} 1/2 & \mathbf{0} \\ \mathbf{0} & 1/2 \end{bmatrix} \begin{bmatrix} \mathrm{b}\boldsymbol{Q}_{11} & \boldsymbol{Q}_{12} \\ \mathrm{b}\boldsymbol{Q}_{21} & \boldsymbol{Q}_{22} \end{bmatrix} \begin{Bmatrix} \boldsymbol{\xi} \\ \boldsymbol{\phi} \end{Bmatrix} \quad (1)$$

Where

ξ	Vector of non-dimensional translational d.o.f.'s
ϕ	Vector of non-dimensional rotational d.o.f.'s
$\boldsymbol{M}_{ij}$	Block matrix terms in mass/inertia matrix
$\boldsymbol{K}_{ij}$	Block matrix terms in stiffness matrix
$\boldsymbol{Q}_{ij}$	Block matrix of aerodynamic terms

The above set of non-dimensional governing equations is simplified based on several assumptions. For instance, they do not included the body forces due to gravity acting on the aircraft (this would require the Froude number be maintained) and assume inviscid, thin airfoil theory (therefore not imposing a hard constraint on the Reynolds number). Though the physics are limited, they are deemed adequate for a low-cost exploration of flight mechanics in real world conditions.

From this set of equations it can be seen that an equivalent system is achieved if the non-dimensional mass, stiffness and aerodynamic terms are conserved $(\bar{M}, \bar{K}, Q)$. Since the outer mould line of the

aircraft is preserved, the aerodynamic terms can be assumed to be preserved as well (recalling the inviscid flow assumption). This leaves only the non-dimensional stiffness and mass distributions to match in order to ensure an equivalent system.

The static mode shapes and non-dimensional frequencies of a system are a direct result of the mass and stiffness distributions. Inversely, if the modal response is matched, the mass and stiffness distributions can be assumed to be equivalent. This is the basis of the scaling process used in this work, the non-dimensional frequencies and mode shapes of the full scale aircraft will be replicated in the reduced scale RPV. This means that the internal geometry of the RPV can be arbitrary, so long as its modal response matches that of the full scaled aircraft.

An arbitrary internal structure is chosen for the RPV and geometric parameters (such as material thickness or locations of trimming weights) are optimized to match the desired modal response. Adding to the challenge is the requirement to create a model that is both flight-worthy and capable of testing throughout the required envelope. In order to reduce the project risk, and distribute the workload over two sets of resources, a flight test program is under development that will deliver rigid (non-aeroelastically scaled), reliable, proven RPV test bed which can be modified to exhibit the desired aeroelastic properties at a later date.

This “rigid” RPV will have the same overall mass and inertia (to closely match the flight dynamics) but neither the mass or stiffness distributions will be matched. The goal is to flight test this RPV before “re-winging” the aircraft with a set of fore/aft wings and tail boom which have been aeroelastically scaled.

This report outlines the detailed design and construction efforts of the rigid prototype as well as the work performed on developing an autonomous control system to be used during flight testing. A brief description of several foreseen issues is given as well as various proposed solutions

1.2 Project Timeline

Rigid aircraft design was performed at the University of Victoria for the early part of 2009, in parallel with further development of the aeroelastic scaling framework. Building of the rigid prototype began in August at the Portuguese Air Force Academy in Sintra, and further building will taking place in a newly formed unmanned vehicles workshop in Victoria starting in the new year.

The building is on schedule for a roll out in early summer 2010 with initial flight testing beginning September, at Ota Air Force Base in Portugal. A detailed flight test plan is being drafted at present by researchers at Virginia tech which will serve the bases of the rigid aircraft flight tests.

1.3 Report Layout

This report will touch on some of the design considerations specific to the rigid RPV and then focus primarily on the building efforts undertaken this past year. Specifically, the sizing of the engines and drag estimates will be discussed, with their implications on flight test times.

The next section introduces the building process. It is split up into subsections relating to each major part or subassembly (i.e. fuselage, wings etc). each of these subsections describes the building that has been done to date as well as work being carried out at present and in the near future.

A section is included outlining perceived challenges in terms of the aircrafts flight dynamics. Here the problems are introduced and three preliminary solutions that are being investigated are proposed. The section which follows briefly describes work that has taken place to develop a 6dof flight dynamics simulator and its integration into “hardware in the loop” simulations being performed to evaluate the proposed modifications and tune the stability augmentation system.

Finally, a brief summary of the work on autonomous control of a trainer aircraft is presented. The purpose of this work is to familiarize our group with the operation of a commercial autopilot while testing analytical models and training pilots/support personnel.

2 Aeroelastic Scaling Efforts

The aeroelastic scaling efforts performed in the early part of 2009 focused primarily on implementing the scaling framework developed previously (1) with higher fidelity models of the joined wing Sensorcraft configuration.

Two methods of scaling were investigated in detail; one which serves to scale the mass and stiffness by matching the supplied modal response in a single optimization loop. The second method involves separating the mass and stiffness optimizations into two separate optimization routines.

The conclusion of the work is that the second method is far superior but with one particular disadvantage. The separation of the mass and stiffness optimization requires additional information about the full scale aircrafts response in the form of static deflection due to a known load. This deflection data is first used to match the overall stiffness before the mass distribution is then tuned by matching the modal data.

Scaling efforts have been put on hold while our group has been waiting for the additional data to be generated and receive clearance. This has not affected our overall project flow as the majority of efforts have been required in designing and building the initial rigid flight test article.

3 Design Work

The detailed design is outlined in previous work (1). However, one aspect of the design procedure is being revisited after concern was raised due to the short flight testing times predicted based on aircraft performance calculations.

The initial flight test profile is included in Figure 1 below.

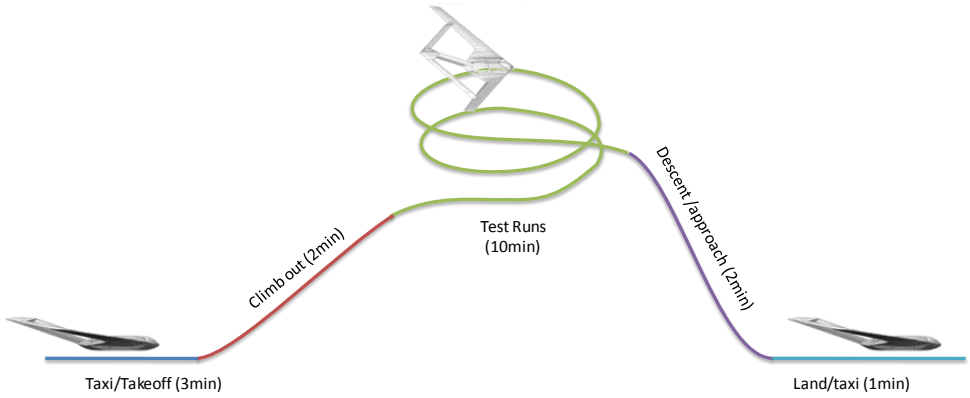

Figure 1 - Mission Profile for Testing Phase

This initial mission profile allows a short 10 minute period for testing which has been pointed out to be insufficient. The reasoning for such a short test window was based on the high fuel consumption calculated from supplied aircraft drag polars (2) and engine specific fuel consumption (3). However, the initial calculations were very conservative since no accurate engine fuel consumption data was available other that the consumption at maximum thrust. Additionally, recent communications with Dr R Canfield suggest that the supplied polars were over predicting drag.

The overall mission analysis needs to be revisited using more accurate data. To date, our group has contacted Jetcat, the manufactures of the P200 engines to be used on the RPV, as well as several modelers with experience using these engines. It is hoped that they will supply thrust specific fuel consumption figures over the whole operating range of the aircraft. If these cannot be obtained, our group has set up a test-stand for testing model turbine engines and will perform tests on these engines in-house.

Figure 2 - Turbine Engine Test Stand to be used for determining TSFC of Jetcat Engines

More accurate data is required for aircraft drag. It is hoped that the USAF ARFL/AFIT and or Boeing will make recent data for Joined-Wing Sensorcraft obtained recently in the NASA AMES wind tunnel tests.

4 Building

This section summarizes some of the building of the RPV that has taken place over the summer. A few of the processes are described as well as a brief description of present/future work.

4.1 Laminate Parts

A variety of laminate sheets are required for producing components such as ribs, spars and bulkheads. All of the required laminate sheets are produced using the Vacuum Assisted Resin Transfer Method (VARTM), some of which are shown in Figure 3 below. This method is a closed process in which the epoxy resin is pulled into a single sided mould by negative pressure, and thereby is distributed throughout the materials previously laid out in the mould. This has several advantages over wet layups and traditional vacuum methods including higher fiber-to-resin ratios and lower void contents.

Figure 3 - Laminate Sheets Produced using VARTM

Since the laminate sheets are planar, a simple flat countertop is used as the tool. The stacking sequence varies per the application but the general procedure is as follows. First the countertop is waxed and then peel ply is laid down, next the layers of fabric are laid down (outermost first) with an outer layer of light glass scrim used as the first layer. Varying layers of carbon cloth are used and then the core material is added. In this case, Airex C70 closed cell PU foam is used with 3mm through holes drilled at 10cm intervals over the entire area of the sheet. These holes allow the transfer of resin through the foam to ensure the fabrics on both top and bottom surfaces are wet out evenly. Next, the stacking sequence of the fabric mentioned earlier is reversed on top of the foam core and finished with a layer of peel-ply. As a final step, a flow medium is laid over the part and the entire laminate is covered in vacuum film. An inlet port is added to one edge of the laminate for the addition of epoxy resin and at the opposite edge of the laminate is located the vacuum port. When a vacuum is drawn, the resin is pulled into the bag and a front of resin is drawn across the laminate as seen in the following figure.

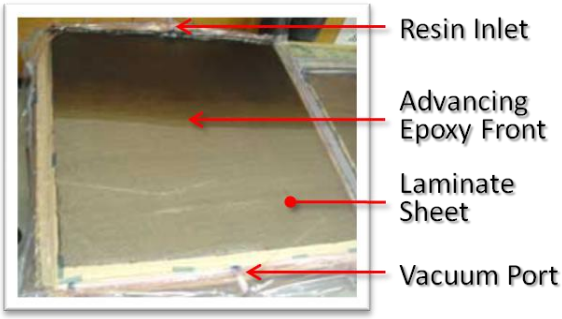

Figure 4 - Laminate Sheet in VARTM Process

When finished, the panels are machined using a diamond tiped tool on a 4'x6' CNC router table. Immediately before using the finished part, the peel ply is removed which ensures a high energy surface which ensures good bonding of parts.

4.2 Fuselage

The fuselage consists of the main body and includes the portion of the forward wing inboard of the break in the trailing edge (as seen in Figure 5 below). The fuselage is common to both the rigid aircraft and the aeroelastically scaled RPV and is defined by the outer mould line supplied for the aircraft.

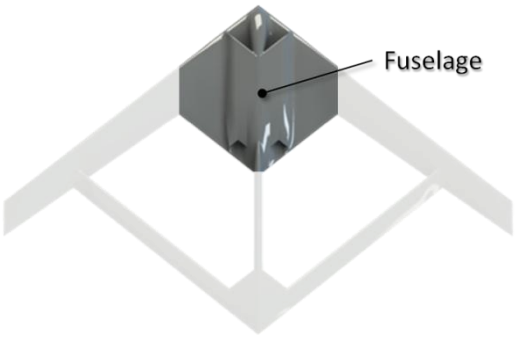

Figure 5 - Fuselage Portion of RPV

4.2.1 Fuselage: Work Completed

The fuselage skins are produced using female moulds constructed using Computer Numerically Controlled machinery (CNC).

Due to the high costs associated with machining, a 3 axis CNC machine is used to produce the positive plugs of the fuselage, rather than a more expensive 5 axis machine that is capable of producing a more accurate result. The maximum working envelope of the machine requires that the fuselage be produced in four parts, the top left, top right, bottom left and bottom right. A low density polyurethane foam is chosen as the plug's material as it is very easy to machine and does not require roughing paths to remove large volumes of material. A large step-over distance (or the distance between successive machining paths) of 8mm is used to further minimize the machining time.

The tool-paths are generated directly from supplied surface data using Catia V5 machining workbench. Figure 6 below shows the generated tool-paths as well as a simulation of the machining process for the top left section of the fuselage.

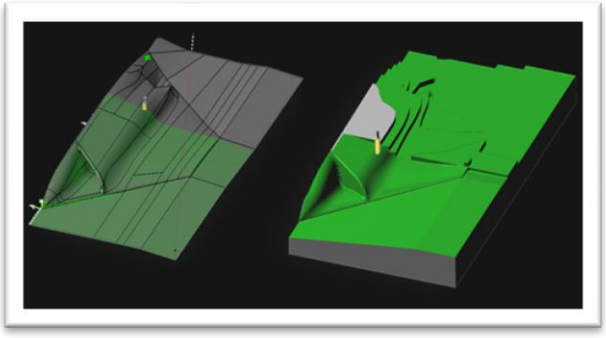

Figure 6 – Tool-paths for Plug and Simulated Machining Pass

The resulting foam plug has large ridges due to the big step over distances used between tool-paths. These ridges are removed using rasps and sandpaper to within and estimated error of +- 1mm from the actual geometry. Figure 7 below shows the plug after sanding is completed.

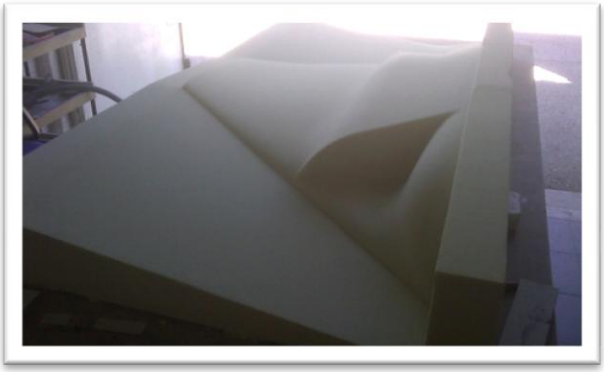

Figure 7 - Foam Plug after Sanding

The resulting plug is quite soft and very porous. Therefore the next step requires sealing the plug. The first step in the sealing process is to fill the pores with a slurry consisting of two-part epoxy resin, thickened with fiberglass microballoon filler to achieve a consistency of catsup (1:1 ratio by volume of epoxy to microbaloons). Once this layer has gelled, another layer is applied and 0.7 oz fiberglass cloth is draped over the part. Peel-ply is applied to the entire surface to prevent the epoxy from flowing and to ensure a suitable surface for the primer to adhere to when cured.

Figure 8 - Application of Micro Slurry to Seal Plug

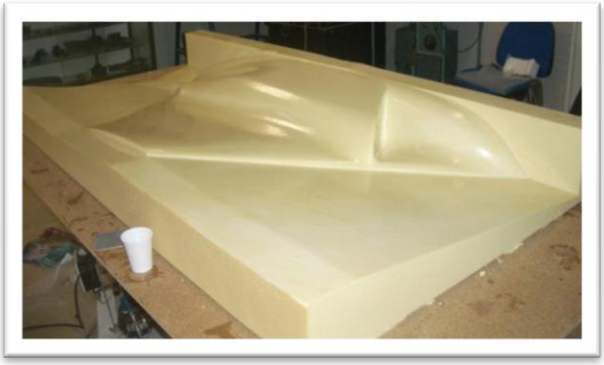

Figure 9 - Plug after Application of fiberglass Layer

Once cured and the peel-ply is removed (see Figure 9 above) three layers of automotive sealer/primer spray paint are applied. This is then sanded to remove any blemishes in the surface. The procedure of painting and sanding is repeated again before final sanding is performed using progressively finer

sandpaper, up to 1000 grit. 10 layers of mould release wax are required for this “green” mould. The resulting plug is shown in Figure 10 below.

Figure 10 - Finished Plug with Vertical Walls Built Around Perimeter

Once final sanding is complete a “wall” is built on the parting plane around the perimeter of the plug (see Figure 10 above). This allows a vertical face to be built into the female moulds that give added rigidity to the final mould, which experiences substantial forces when the parts are formed using vacuum processes. The final step is to lay up the female moulds on the finished plugs

This is achieved by first applying two coats of epoxy based gel-coat to the plugs. After gelling, chopped fiberglass strand is filleted into sharp corners and recesses on the plug. A layer of 1.4 oz fiberglass cloth and epoxy is then applied and allowed to gel. Next two layers of 2 oz fiberglass matt and epoxy are applied and allowed to gel. This process is repeated with two more layers of matt and once gelled, a final layer of 1.4 oz cloth is applied. The resulting mould is quite thick (~8mm) which necessitates applying layers a maximum of two at a time in order to reduce the risk of the epoxy exotherming. Figure 11 below shows the female mould curing on the male plug while Figure 12 show the same mould after being removed from the plug.

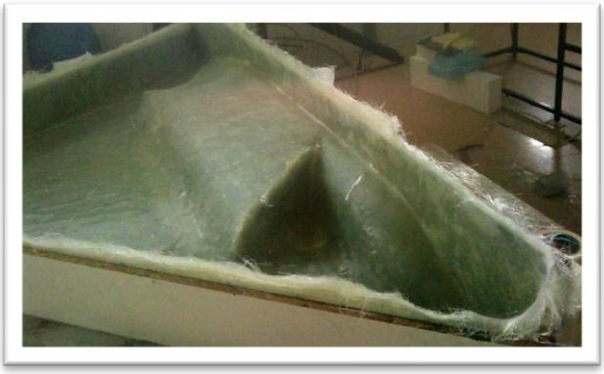

Figure 11 – Fiberglass Female Mould Curing on Plug

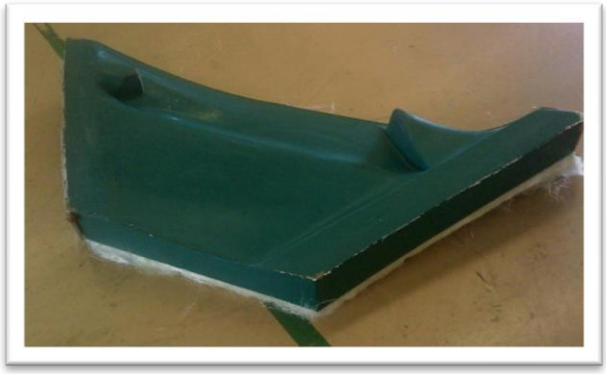

Figure 12 – Female Tool after Removing from Plug

The last stage of the mould's construction is to bolt the left/right halves of the moulds together. They are then mounted to a steel frame and shimmed in order to ensure the geometry coincides with that of the original (ie no twist or bending in the moulds). These moulds are then ready to lay up the fuselage skins which will be described in the following Future Work section.

The internal structure of the fuselage consists of bulkheads made of laminate sheets formed using VARTM techniques as described in section 4.1. The bulkheads are cut out using 2d contour passes on a CNC router table and all interlock with one another to ensure accurate locating of the parts as shown here.

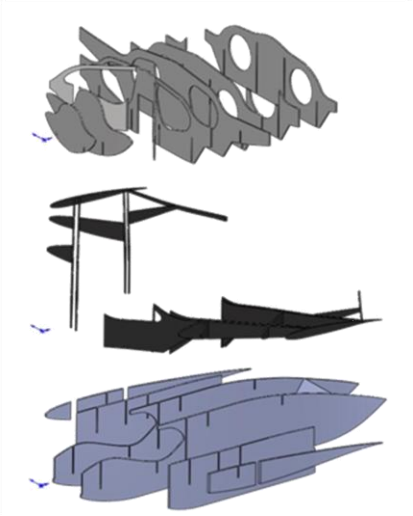

Figure 13 - Exploded View of Fuselage Bulkheads

4.2.2 Fuselage: Future Work

The next stage in constructing the fuselage is producing the skins using the completed moulds. The skins will consist mainly of two layers 0.73 oz/yd^2 fiberglass and +-90^o 5.6 oz/yd^2 carbon plain weave cloth. The main load paths are carried from the wing through the spar-caps imbedded in the fuselage skin that tie into the swept bulkheads in the inner wing section of the fuselage (seeFigure 14). At these locations the skin will be reinforced with layers of 4.7 oz unidirectional carbon. Additional reinforcements will be required at various points such as access panel openings.

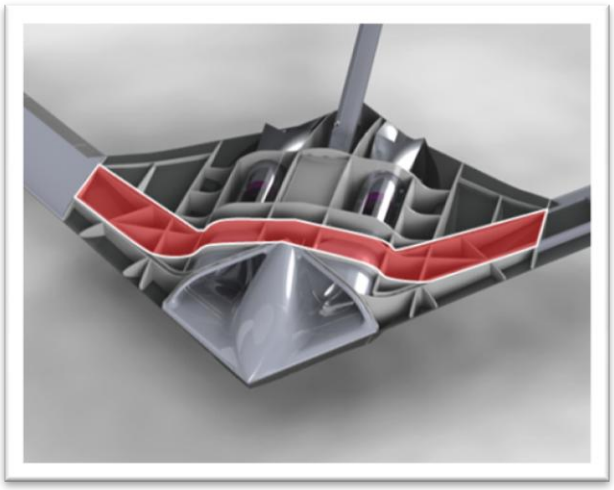

Figure 14 - Location of Unidirectional Reinforcement in Fuselage Skins (Top Skin Shown in Red)

Once the skins are laid up the bulkheads are set into the lower skin and filleted into the skins using epoxy thickened with glass antisag. A bead of thickened epoxy is then applied to the exposed upper edges of the bulkheads and the upper skin (and upper female mould) is placed on the lower skin/bulkhead assembly. The whole assembly is placed under vacuum to ensure proper contact between the skins and the bulkheads. Additional reinforcements will be applied after the curing to critical areas such as the leading edges of the fuselage.

The preceding description is a very simplified explanation of the process but serves to familiarize the reader with the general methods used.

4.3 Fore/Aft Wings

The fore and aft wings for the rigid prototype are produced using male tooling. In other words, a foam core is produced for the wing and is then used as the tool to build the outer composite skins. When the skins are completed, the foam plugs can either be removed (by dissolving them using acetone for instance) or else left in the wing to add strength and prevent skin buckling. In the case of both the fore and aft wings, the foam cores will be kept for increased rigidity.

4.3.1 Fore/Aft Wings and Boom: Work Completed

The wing construction can be seen in the following figure which shows a cross section of the aft wing and its control surface.

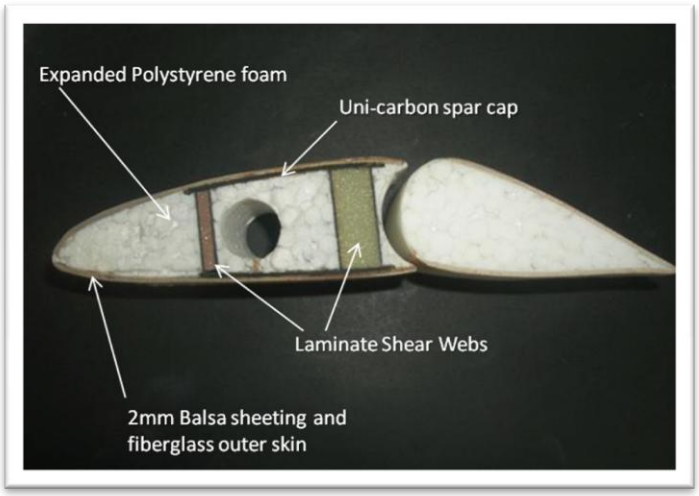

Figure 15 - Cross Section Showing Wing Structure

The main wing is cut in eight panels along the length of the wing in order to accurately capture the changing wing cross section along the span. The rear wing is assumed to have a linear twist and therefore the majority of the rear wing is cut as one piece but due to the large taper ratio of the inboard aft wing section, the panel had to be split in two sections along the chord. Figure 16 shows how the wings are segmented when producing the constituent panels.

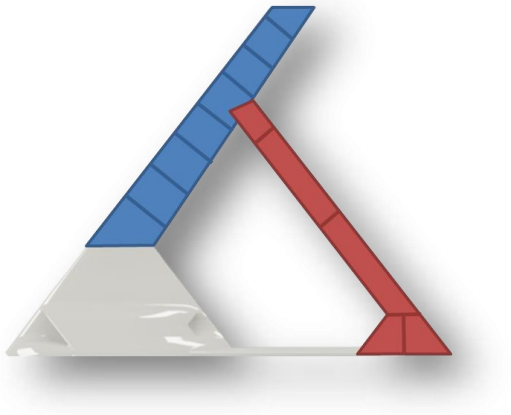

Figure 16 - Individual Foam Panels for Fore/Aft Wings

The foam plug, which acts as the male tool for the wing, is produced using airfoils extracted from the supplied CAD geometry. It is cut from 1.2 lb/ft^2 expanded polystyrene (EPS) foam using a four axis CNC, hotwire foam cutter. Figure 17 below shows the CNC tool path for a typical wing section.

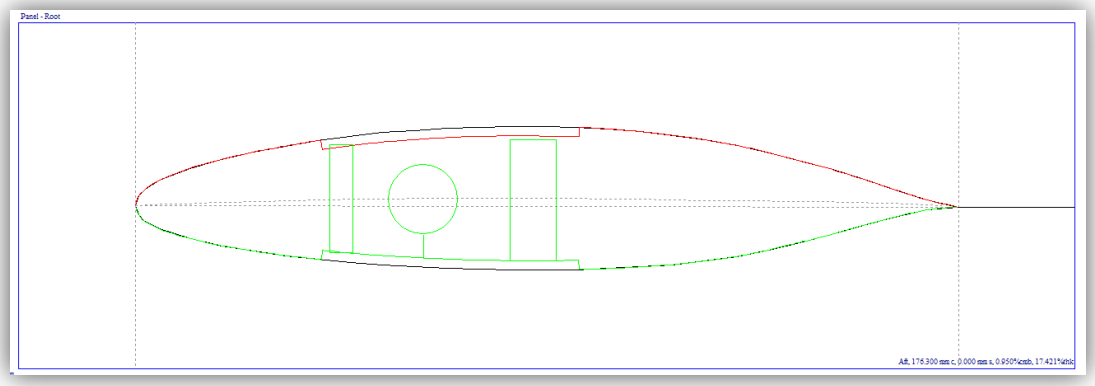

Figure 17 – Hot Wire Tool-Path for Typical Wing Section (Mid-span of Aft Wing in this Case)

In the above figure we can see the typical features of the foam core. The top (red) and bottom (green) surfaces are offset by the thickness of the balsa skins that will be bonded to the outside of the foam. Both surfaces also have a depression cut into them to make room for the spar caps. There are also cut outs for vertical shear webs that connect the upper and lower spar caps as well as an annular conduit for passing servo wires and leads to other electronics such as accelerometers or strain gauges. Figure 18 below shows the cutting process using the 4-axis foam cutter.

Figure 18 - CNC Hot Wire Cutting Wing Profile

Structural components, such as shear webs and wing ribs, are constructed using carbon-foam-carbon laminate (see section 4.1). These critical components are cut using a CNC router. The accuracy of these parts is especially important in areas such as where the aft wing spars join into the main wing as they help to ensure the proper mating of the parts and ensure that the overall geometry is maintained. The figures below show an example of one of these critical CNC cut parts at the end of one of the rear wing shear webs which mates in with the forward wing section.

Figure 19 – End of Rear Wing Shear Web that Joins with Forward Wing

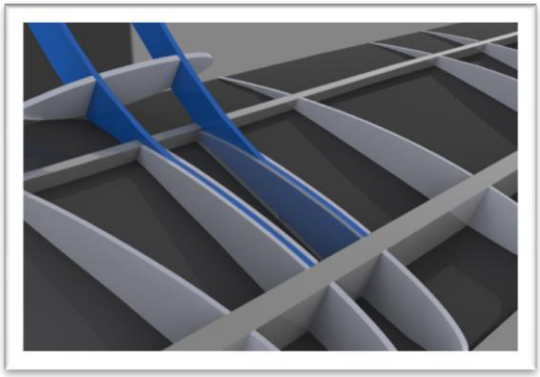

Figure 20 – Same Part, Show in Blue, Connecting the Rear and Forward Wing

The laminate shear webs are bonded into the foam cores along with other structural items such as wing joiners (tubes which accept wing-joining rods) and hard-points for control surfaces. These cores then act as a male tool forming the spar caps and wing skins using vacuum forming techniques. The EPS foam is quite porous and therefore the recess for the spar-cap is sealed using a layer of thickened epoxy. This ensures that when the spar caps are vacuum formed into the recess, they have a hard, flat surface to bond to (this ensures that voids between laminate layers are minimized and that excess epoxy is not driven into the foam). Figure 21 shows a foam core ready for vacuum bagging.

Figure 21 - Aft Wing Foam Core Ready for Vacuum Bagging

The spar caps, which consist of layers of 4.7 oz/ft^2 unidirectional carbon between two layers of ±45^o Carbon cloth, are laid up with epoxy in the recesses in the upper/lower surfaces of the foam core (see Figure 17 above). The overall thickness of the spar cap corresponds to the depth of the recess in the foam so that the spar cap comes flush with the foam's surface. The entire core is then sheeted in 2mm balsa which has been scored along the grain (this ensures that any excess resin and air pockets in the

spar cap layup is driven out through the balsa rather than remaining in the layup). This whole assembly is then placed under vacuum to cure.

When the wings have cured, the balsa sheeting is sanded to fair the surface and a final layer of fiberglass veil is applied to seal the surface for painting. Two layers of sand able primer are applied and sanded in preparation for final painting after the final assembly is completed. An example of a completed surface is shown in the following figure.

Figure 22 - Completed Tail Boom

4.3.2 Fore/Aft Wings and Boom: Future Work

Work to date has seen the completion of the aft wing and boom layups. The front wing will be built in the New Year and then the post operations will be completed on the wings. This includes cutting the control surfaces from the wings and attaching them with hinge points. The servo openings will be cut into the wings and linkages added.

4.4 Intake/Exhaust routing

Since the fuselage skins are made using a female tool, no negative draft angles can be present. This necessitates the use of separate tooling for the air intake and exhaust outlet pass troughs. Figure 23 shows the locations of the outer mould line which cannot be produced using the female fuselage moulds alone (skins produced using the female fuselage tooling described in section 4.2 shown in gray). Both the inlet and outlet (shown in yellow and red respectively) require their own separate tooling.

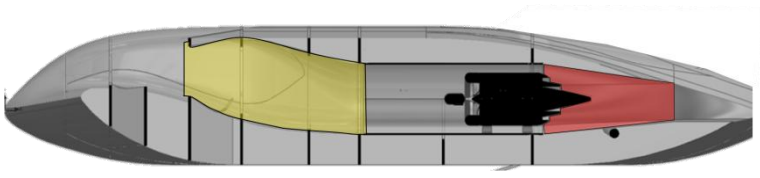

Figure 23 – Intake/Outlet Skins Requiring Their Own Separate Tooling.

This tooling is produced as a male plug or mandrel that a composite skin is laid up on. Due to the complex shapes of the inlets and outlets the part cannot be removed from the mandrel without cutting it off. The parts are cut down their length and then re-bonded after removing from the mandrel.

Due to the complex shapes of these tools, they are constructed using many 2d contours stacked on one another and then sanded to a fair surface. This foam core is then sealed with layers of fiberglass and finished with primer.

Figure 24 - Male Plugs Used for Producing Air Intake Skins (left) and Outlet Skins (Right)

The hot exhaust gas leaving the engines must be routed through the outlet while still allowing cooling air to flow around the engines. Figure 25 shows how the cooling air passes over the engine and exits the outlet while the hot air is routed out through an insulated exhaust tube (shown in the figure as silver section).

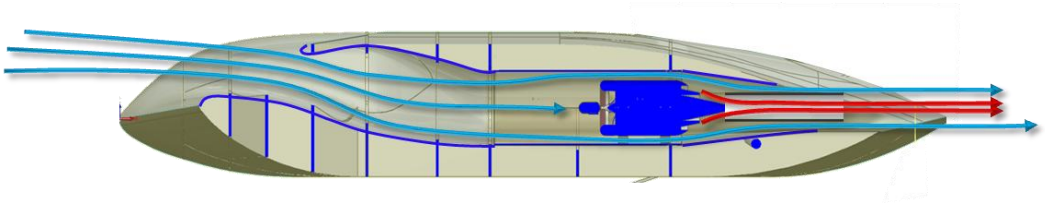

Figure 25 - Cross Section Showing Engine Locations, Inlets and Exhaust Routing

This exhaust outlet must be insulated in order prevent damage to the composite fuselage. It is constructed as a double walled tube with a corrugated internal structure. The material is titanium and an example is shown below.

Figure 26 - Double Walled Exhaust Pipe

5 Stability and Control Issues of RPV

A detailed analysis of the joined wing flight dynamic stability was carried using Vortex Lattice Methods (VLM) by the author in a previous work. These initial investigations were performed using HASC (High Angle of Attack Stability and Control) software to determine dynamic stability and control characteristics for developing a 6dof simulator. Additional analyses were also performed using Athena Vortex Lattice code developed by Mark Drela et al at MIT. Results from both analyses showed very close agreement and as a result the majority of subsequent analyses are performed with AVL due to its more robust inputs and user interface.

There are two main motivations for further investigation of the flight characteristics. The first is that the initial analysis showed that the aircraft had marginal yaw stability and it may be necessary to modify the initial aircraft to reduce or eliminate this. The second motivation is that the present configuration does not have a rudder surface and some form of yaw authority is required, whether through scheduling of other surfaces or the addition of a new surface on which to include a rudder.

The following sections introduce the baseline results as well as three alternate configurations and methods to improve yaw stability while introducing a form of control authority. It should also be noted that unless otherwise stated, all results specified are for the flight condition specified in Table 1 below.

Table 1 - Reference Quantities Used in Subsequent Analyses

Reference Quantity	Symbol	Value	Units
Planform Area	S	1.39	m^2
Mean Aerodynamic Chord	$\bar{c}$	0.404	m
Span	b	5	m
Air Density/Altitude	ρ/Alt.	1.180/400	Kg/m^3, m

The mass properties assigned to the aircraft correspond to the supplied full scale test point after having been scaled by the derived scaling factors to map them to the reduced scale test point.

5.1 Baseline Aircraft

The baseline configuration is defined by the supplied CAD geometry of the aircraft. Since no control surfaces are specified from the given geometry, the following control surface layout is used for the present work. Figure 27 shows the chosen locations and the numbering of the control surfaces.

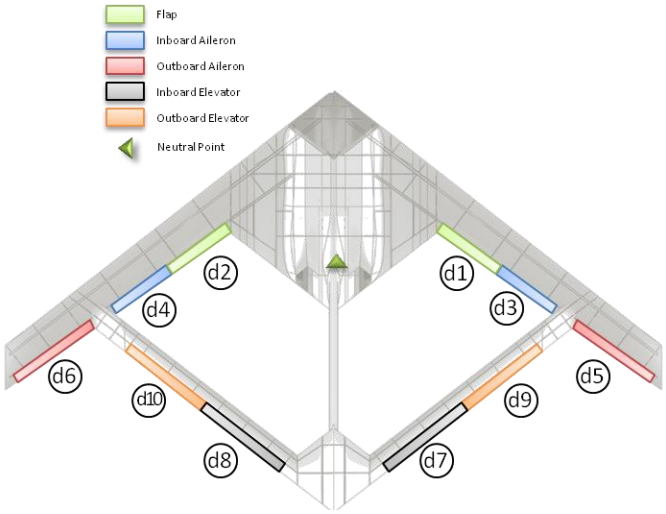

Figure 27 - Control Surface Locations and Numbering

Figure 28 below shows the discretized baseline geometry. The large figure on the left is a representation of the geometry with the airfoil thickness' rendered along with the control surfaces. The top right model is the HASC geometry and the lower right shows the model used with AVL.

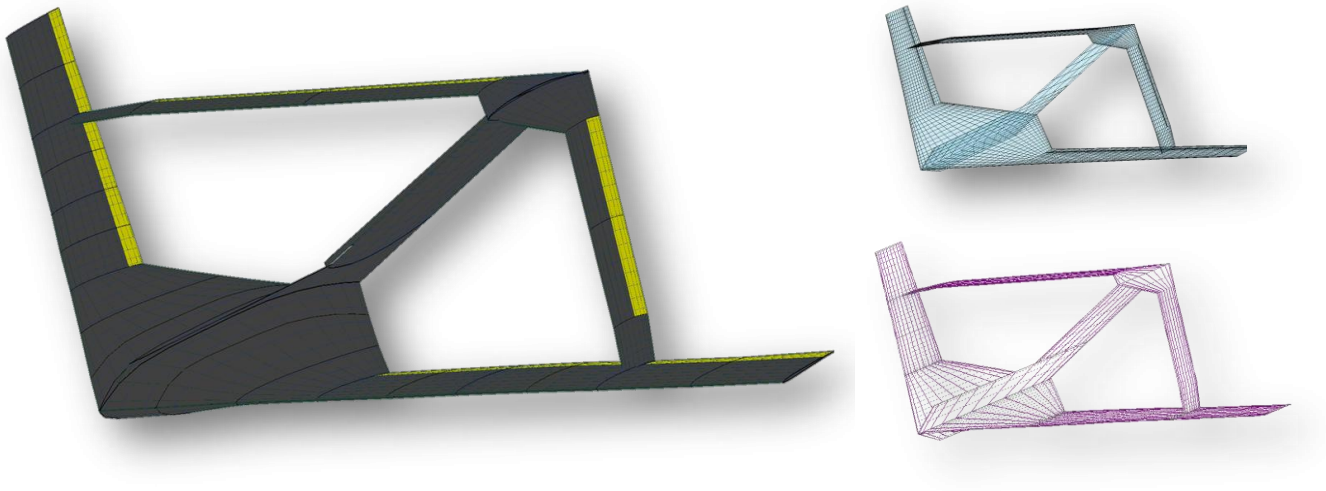

Figure 28 - Vortex Lattice Models of Baseline

The stability derivatives resulting from the analyses are included in Appendix 1. These stability derivatives, along with the scaled mass properties of the full scale aircraft, are used to compile the state

space model of the aircraft. A subsequent analysis of the decoupled lateral/longitudinal sets of equations yields the following results.

Table 2 - Dynamic Stability for Baseline Configuration

	Eigenvalues		$T_{1/2}$	$n_{1/2}$	Period	freq.	ζ	ω_n	τ
Mode	real	Im	sec.	-	s	$^1/_s$			
Phugoid	-4.34E-03	0.4621	159.756	11.719	13.596	0.074	0.009	0.462	
Short Period	-2.92181	2.8577	0.237	0.108	2.199	0.455	0.715	4.087	
Dutch Roll	6.19E-02	1.6562	11.200	2.944	3.794	0.264	-0.037	1.657	
Roll	-4.65472	0	0.149						0.214836
Spiral	-3.76E-02	0	18.446						26.61826

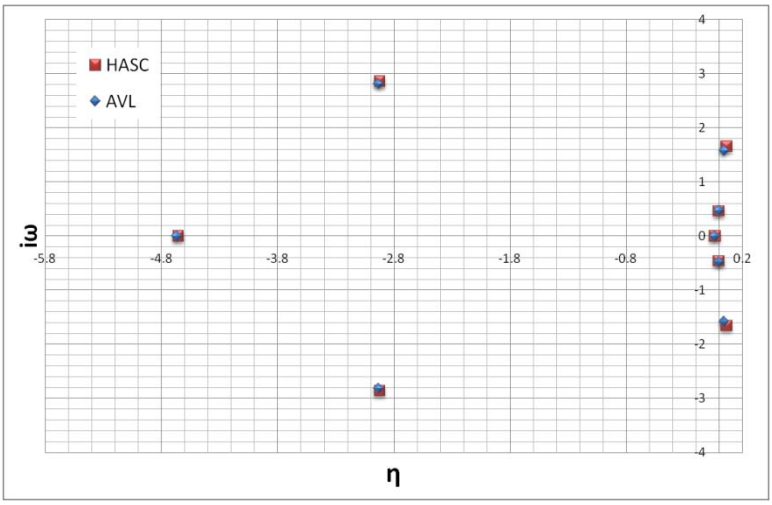

Figure 29 - Eigenvalues of Baseline Geometry

The results show that all modes are stable with the exception of the dutch roll mode. Flying qualities are rated based on the guidelines outlined in Ref (4). All of the modes achieved highest rating for flying quality, level 1, in all categories of flight with the exception of two. The dutch roll mode is unstable and the phugoid mode only achieved level 2 rating in all categories (A, B and C).

The level 2 rating is defined as having *"Flying qualities adequate to accomplish the mission Flight Phase, but some increase in pilot workload or degradation in mission effectiveness, or both, exists".* It may be the case that a level 2 flying quality in the case of the phugoid mode is not of large concern to the RPV pilot, especially since the perceived flying qualities for small unmanned aircraft can be quite different from that of full scale aircraft. Of greater concern however is the instable dutch roll mode. The following design modifications are proposed as possible solutions to this problem.

5.2 Proposed Modifications

Three solutions are investigated here to deal with the lack of yaw stability and control authority.

5.2.1 Addition of Vertical Surface with Control Surface

The first solution involves the addition of a vertical tail surface aft of the tail boom and this surface is fitted with a control surface. Figure 30 below shows the AVL model modified with this additional surface.

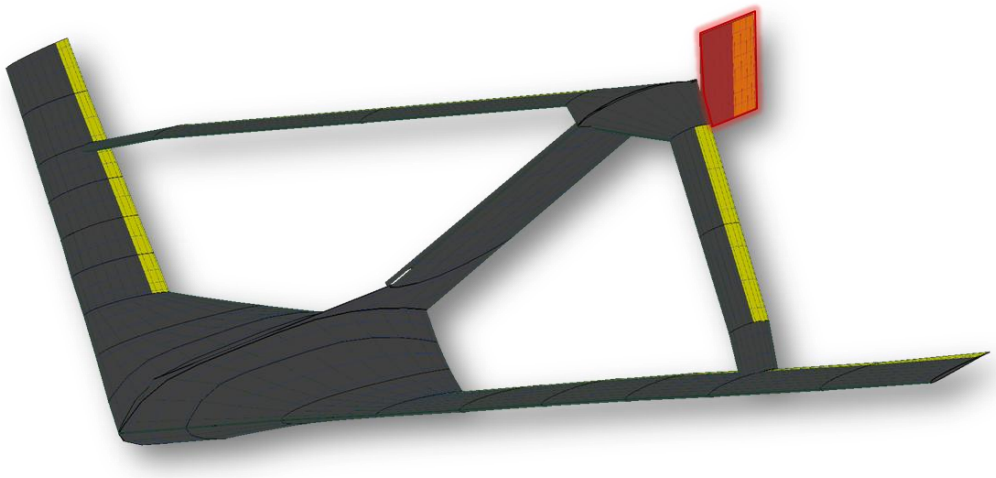

Figure 30 - Configuration with Vertical Tail Surface

An analysis performed on this configuration shows its effectiveness at damping out the dutch roll. The addition of the surface improved the dutch roll mode to a level 2 flight quality while adding sufficient yaw authority. The other modes see little change as a result of this modification with the exception of the spiral stability mode which sees a drop in its time to double amplitude. The spiral stability mode does however maintain a level 1 quality rating.

Table 3 - Dynamic Stability for Configuration with Addition of Vertical Surface

	Eigenvalues		$T_{1/2}$	$n_{1/2}$	Period	freq.	ζ	ω_n	τ
Mode	real	Im	sec.	-	s	$^1/_s$			
Phugoid	-4.34E-03	0.4621	159.756	11.719	13.596	0.074	0.009	0.462	
Short Period	-2.92181	2.8577	0.237	0.108	2.199	0.455	0.715	4.087	
Dutch Roll	-6.81E-02	2.0564	10.171	3.320	3.055	0.327	0.033	2.058	
Roll	-4.65472	0	0.149						0.214836
Spiral	-3.07E-02	0	22.598						32.60913

This modified configuration will undergo testing using the 6dof flight simulator (to be introduced in a later section) to assess its overall effectiveness. The goal is to have the pilot (Capt. Jose Costa, Portuguese AFA) fly this, and all other proposed configurations, in the simulator and asses it based on the Cooper-Harper Pilot Rating Scale (4).

One potential drawback of this modification is its effect on the aeroelastic response of the aircraft. The addition of this surface has an effect on the lateral aerodynamic modes which may play a role in the aeroelastic modes, especially those which have similar frequencies to these rigid body modes.

5.2.2 Addition of Conventional Tail Boom

The pilot who will be operating the RPV has voiced some concern about the amount of pitch authority that will be available to the aircraft. The VLM analysis shows adequate authority is available but it may be desirable to include modifications to the early flight vehicle just in case. At a recent meeting at Virginia Tech., LTCol Shearer and Maxwell Blair from USAF ARFL/AFIT suggested the addition of a conventional tail boom to the initial flight test article. This would add additional pitch authority from an elevator surface mounted to the new horizontal surface, while also adding the benefits described in the previous section. Figure 31 below shows the proposed modification to the baseline configuration.

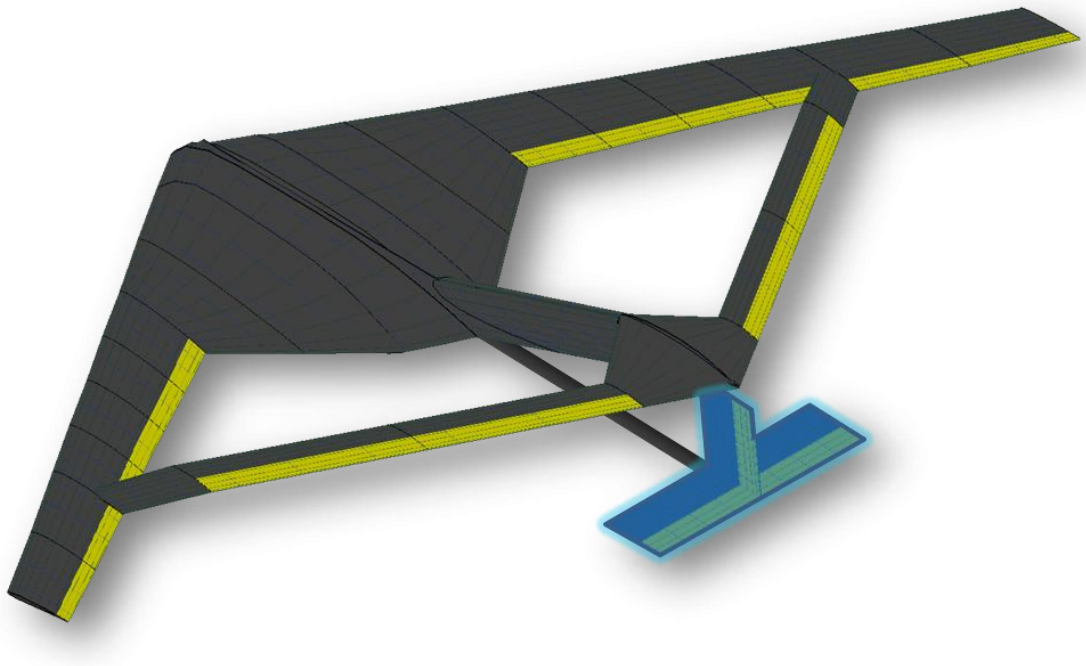

Figure 31 – Configuration with Addition of Conventional Tail Surfaces

An analysis performed on this configuration shows the dutch roll mode is made stable although only to a quality level of three. This is due to the fact that the tail, although the same size as in the previous case, is at a shorter distance from the cg. A further improvement is possible through increasing the size of the vertical stab and/or increasing the boom length. The other modes are affected by a small degree but not enough to affect their flying quality ratings. The phugoid mode was improved however but is still rated level 2. The results of this analysis are shown in Table 4 below.

Table 4- Stability for Configuration with Addition of Conventional Tail Surfaces

	Eigenvalues		T1/2	n1/2	P	f	ζ	ω_n	τ
Mode	real	Im	sec.	-	s	1/s			
Phugoid	-5.35E-03 ±	0.4582	129.431	9.413	13.714	0.073	0.012	0.458	
Short Period	-3.25378 ±	2.8376	0.213	0.096	2.214	0.452	0.754	4.317	
Dutch Roll	-6.63E-03 ±	1.7277	104.551	28.672	3.637	0.275	0.004	1.728	
Roll	-4.67633 ±	0	0.148						0.213843
Spiral	-3.70E-02 ±	0	18.746						27.05026

This modified configuration will undergo testing using the 6dof flight simulator to assess its overall effectiveness. The effect of the tail will likely need to be increased by increasing the size of the surfaces and/or increasing the length of the tail boom.

The same potential drawback arises for this configuration that did with the previous. Making large changes in the aerodynamics will have an effect on the aeroelastic response of the aircraft. This is even more drastic with the addition of the horizontal surface as it will affect the pitch/plunge of the aircraft in flight. Another potential drawback that must be investigated is the added mass at such a large distance aft of the cg. This may be difficult to account for in trimming the aircraft

5.2.3 Active Control Using Existing Surfaces

The final solution involves scheduling the existing surfaces to gain some level of yaw authority which can then be used with an active yaw damping system. Yaw damper systems are quite common with RC aircraft and can be purchased inexpensively off the shelf. Their operation varies but most consist of a unit which is place in series between the remote receiver and the rudder servos. Some units also allow mixing of multiple surfaces for yaw control such as with y-tails.

Another option is to use stability augmentation via the autopilot unit. When in autopilot mode the yaw is damped using the built in feedback loops, but the concern is in the flight regimes where the pilot is flying the aircraft in manual mode. The Micropilot 2128^{LRC} autopilot (the autopilot chosen for this aircraft, see section 7: Autonomous Control) has a built in yaw damping feature which allows the pilot to control the aircraft remotely via and RC controller while automatically mixing in rudder commands to damp out unwanted yaw.

In order for these solutions to be effective and robust, an adequate degree of yaw authority is required. If no modifications are made to the geometry then the yaw control must come as a result of deflecting a combination of the existing controls. This is proposed in several ways.

The first scheme involves deflecting the outer aileron down and outer elevator up on one wing. The amounts for each deflection have to be chosen so as to minimize the effect on motion about the other axes, while achieving the required yawing moment. The effect on the roll is twofold; first, the increase in drag caused by the deflected surfaces acting at a distance outboard of cg causes a yawing moment. The second effect is caused by the resolved components of lift in the spanwise direction due to the dihedral/anhedral of the wings. This effect is shown in the following figure.

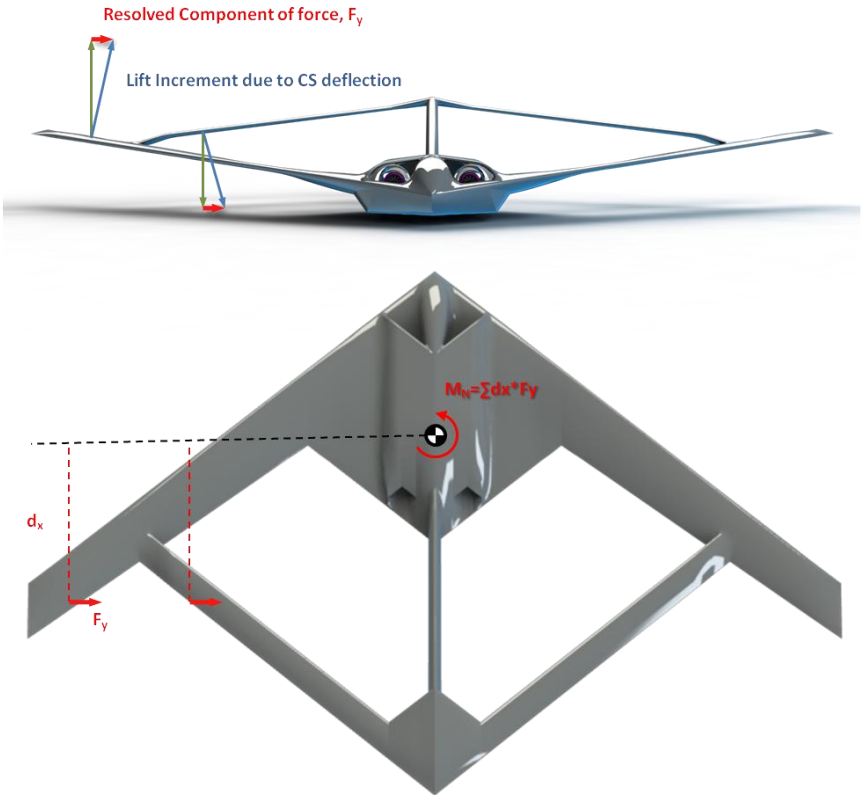

Figure 32 - Effect of Resolved Lift Increment on Aircraft Yaw

In order to ensure that the yawing moment resulting from these control surface movements is uncoupled from the other aircraft degrees of freedom as much as possible, an optimized combination of deflections is desired. Present work is focused on finding this combination of deflections and quantifying their effect using a 6dof flight simulator.

This solution has the added benefit that it does not affect the stick fixed aerodynamics of the aircraft. Potential drawbacks however are the added complexity of advanced scheduling schemes and the danger of flying an aircraft that is potentially unstable.

Further work is focusing on further analyzing and refining these proposed modifications and quantifying their effect in simulations. It is also hoped that some additional information will be made available to our group in the form of aircraft data, such as stability derivatives calculated with higher fidelity methods or compiled from wind tunnel tests. These challenges further emphasize the need for a well planned, incremental flight testing plan.

6 Flight Simulator

A 6dof flight simulator has been developed previously by this group within the Simulink modeling environment. The simulator is based on a set of block included in both the Matlab Aerospace Block set and the Unmanned Dynamics Aerosim v1.2 Block set. The previous version of the simulator modeled the aircraft using a set of first order terms. For example, the lift coefficient would be modeled as

$$C_L = C_{L0} + C_L^{\alpha} \cdot \alpha + C_L^{\delta_f} \cdot \delta_f + C_L^{\delta_e} \cdot \delta_e + \\ + \frac{c}{2V_a}\left(C_L^{\dot{\alpha}} \cdot \dot{\alpha} + C_L^{q} \cdot q\right) + C_L^{M} \cdot M$$

The existing model has been subsequently altered to allow non-linear aerodynamics to be modeled through the use of multi-dimensional lookup tables. This allows coefficients to be input for various angles of attack and sideslip angles.

A parametric model is developed using Phoenix Integration's Model Center Software (MC). This model includes the vortex lattice software, AVL that is described in the proceeding section. The MC model runs the AVL analysis through an array of angle of attack and sideslip values. It then parses all the output data and compiles the coefficient arrays into a Matlab m-file. This resulting m-file is in a format that is required by the simulator to initialize an aircraft model. The end result is that modifications can be made to the aircrafts configuration, in the AVL input file, and the new aerodynamics will be simulated in the flight simulator in a matter of minutes. This will allow rapid investigation of design changes by both the engineer and the pilot.

The simulator calculates the aircraft states and then outputs this to a commercial flight simulator for visualization (FlightGear and X-Plane 8 have both been used here). A custom block has also been created that allows the pilot to control the aircraft using an actual RC controller attached to the computer through the "training" port available on most RC transmitters. Figure 33 shows a typical flight simulation with the Simulink model, custom gauges and FlightGear all running simultaneously.

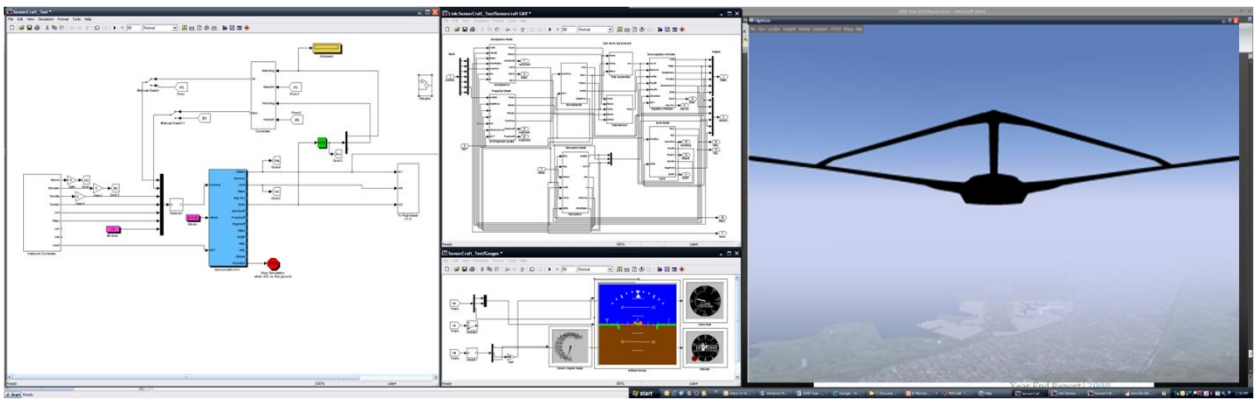

Figure 33 - 6dof Flight Simulator

This Simulink model is also used to investigate the effectiveness of stability augmentation such as a yaw damper. This is taken one step further as a hardware in the loop setup has recently been acquired that allows the actual aircraft autopilot to be incorporated into the simulation.

The Micropilot 2128 THWIL system uses data acquisition hardware to interface the 2128 autopilot within the simulation. Micropilot supplies their own Simulink model to achieve this but this has been modified to replace their physics model with the one developed by this group. The hardware in the loop setup was used to determine a set of PID gains for initial autonomous flight of a trainer aircraft (to be introduced in proceeding section) and to train the pilots and ground crew. In the New Year, the hardware in the loop set-up will be used to investigate the proposed modifications for improving the aircraft stability.

7 Autonomous Control

There are many reasons why it is desirable to integrate a level of autonomy into the initial flight test article. The first is the ability to provide mixing functions as is required for this aircraft, especially if yaw is to be achieved with a mix of ailerons and elevators. Also, this allows flight tests to be performed at smaller or even negative static margins. Another large benefit is an increase in operating range. If fully autonomous, the aircraft can be operated at or outside the limits of visual range. Even if the flights are performed manually within visual range, the ability to switch the aircraft to autonomous mode increases the safety since it can be programmed to return to home, enter a holding pattern etc. The autopilot can also be programmed to deploy a parachute or even ditch if leaving pre-programmed safe operating limits.

Perhaps the greatest benefit is the integration of so many required features into an off the shelf, industry tested unit. even if no level of autonomy is required, the aircraft will still need a suite of sensors including accelerometers, air speed indicators, a GPS system, telemetry and data-logging to name a few. A commercial autopilot has all of these features, and more fully, integrated.

Several commercial autopilots were considered with the final choice being the Micropilot 2128LRC. The LRC stands for Long Range Communications which involves the ability to control the aircraft through redundant, 1 Watt, 900MHz data link. An additional safety feature is the ability to revert the aircraft to conventional RC control through a separate RC Transmitter and receiver. This additional layer of redundancy is very important for this project in terms safety and the cost associated with loosing an aircraft. Additional features of interest that are specific to the Micropilot are the 16 integrated, 20Hz analogue to digital input channels. These will be useful when the aircraft is instrumented with all of the sensors required to monitor the wing deformation for instance.

7.1 Initial Autonomous Flight Tests

As an incremental step, the autopilot is integrated into an existing commercial RC trainer aircraft. The “Senior Telemaster” is well known in the model aircraft circles as an extremely effective trainer with docile flying qualities. The large size (94” wingspan) allows sufficient payload capacity for the autopilot, onboard camera and an oversized fuel tank. Figure 34 shows the Telemaster aircraft used for this work.

Figure 34 - "Senior Telemaster" Trainer Used For Initial Autonomous Testing

A dynamic stability analysis was performed on the trainer and the results used to generate a flight dynamics model in the simulator. The airplanes flight dynamics were linearized around the trim point and an optimization of the feedback gains was performed using the Matlab Control Systems and Optimization Toolboxes. These feedback gains were then uploaded to the autopilot and tested in the hardware in the loop simulator.

The resulting control gains were then programmed to the autopilot onboard the trainer and a series of incremental flight tests were flown in Ota, Portugal at the end of October this year. An initial set of flight test were performed under manual control to characterize the aircraft before an autonomous flight was performed. This initial flight test navigated between a given set of GPS waypoint and the aircraft demonstrated excellent flight qualities. This validated the effectiveness of simulating and tuning the PID gains before initial testing.

Figure 35 show several pictures taken from the initial autonomous flights. Clockwise from the top we see the aircraft in flight. Next is a real-time synthetic display of the aircraft in flight, followed by the ground control software and finally a piece of real-time footage taken from the on-board, gimbaled camera.

Figure 35 – initial Autonomous Flight

After several initial flights, the PID gains were adjusted in-flight by systematically isolating each individual control loop (for instance, elevator position from pitch feedback). During one of these tests, the aircraft wing-joiner broke in flight due to a high g pitch-up maneuver. This resulted in the destruction of the trainer; however, no damage was inflicted on the autopilot or supporting systems. Closer inspection of the aircraft post flight revealed that the wing joiner was made of poor quality materials and the next aircraft has been fitted with a carbon wing joiner and wing struts. The reason for the high g pitch up maneuver was determined from the telemetry. For one of the PID tuning flights the throttle is set to manual override and the autopilot is instructed to climb to an intentionally unachievable level. Unfortunately, the target altitude was set too low and the aircraft achieved the altitude, overshot it and changed its command state to descend back to the target altitude. Since the autopilot had no control over the throttle, the speed increased do a very high level and upon reaching the desired altitude and pitching up to level off, the aircraft experienced high wing loading.

A new flight test program will be undertaken in the New Year with a new trainer model and will take place in Victoria. It is hoped that this will further increase our group's familiarity with autonomous flight while also providing a means to help develop an effective flight testing plan for the initial Sensorcraft tests. A flight test program is being developed by Tyler Aarons et. Al. of Virginia Tech and the goal is to apply their test plan to the trainer aircraft before applying it to the Sensorcraft flight tests. This will allow everyone to work out any unseen issues in the test plan, while serving to train all of the ground crew and support staff involved.

Our group has recently designed and is now building a mobile command center, which will contain the ground control station, communications, regulated power and other supporting equipment for flight testing. Figure 36 shows the 14'x7' trailer to serve as the basis for the mobile command center as well as a rendering of the final concept.

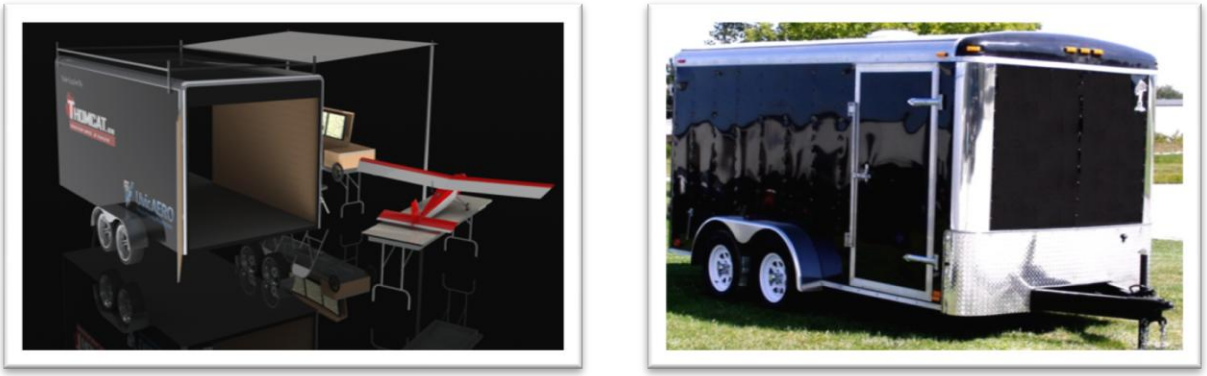

Figure 36 – Mobile Command Center Concept and Trailer

8 Conclusions and Recommendations

Good progress is being made towards the development of the first, rigid remotely piloted vehicle. Construction of the test article is well underway and a newly developed facility in Victoria will soon be operational where building can continue into the New Year. Many of most difficult and time consuming tooling is completed for the aircraft and many critical parts have been built or are nearing completion. The building of the aircraft is on track for completion in July of 2010 with initial flights to commence at the end of the summer at the Portuguese Air Force Base in Ota.

Several issues remain with regards to the stability and controllability of the aircraft. Several methods are proposed to address these potential problems. Their suitability is being explored analytically and qualitatively through the use of a Simulink flight simulator and hardware in the loop simulations. **Additional information, in the form of aircraft polars and stability derivatives from wind tunnel data and/or higher fidelity studies, would aid greatly in the accuracy and effectiveness of these studies. Any assistance we can receive on this front from either AFIT/ARFL and/of Boeing would be of great help.**

Finally, the integration of a commercial autopilot into a trainer aircraft was completed in October of this year. This aircraft successfully navigated GPS waypoint autonomously but later crashed while tuning the feedback gains. The autopilot was undamaged however and a new aircraft is being built. The test flight program of this trainer aircraft is set to recommence in Victoria in the new year. It is hoped that this aircraft will also serve to "dry run" the Rigid Sensorcraft's flight test program in the spring, which is presently being developed at Virginia Tech.

9 Works Cited

1. ***Richards, Jenner.*** *2008 Progress Report. Victoria : University of Victoria, 2009.*

2. ***Bond, Vanessa.*** *FLEXIBLE TWIST FOR PITCH CONTROL IN A HIGH ALTITUDE LONG ENDURANCE AIRCRAFT WITH NONLINEAR RESPONSE: Dissertation Prospectus. Dayton : AFIT, 2006.*

3. ***Jetcat Germany.*** *Jetcat Products/Turbojets/P200 . Jetcat Germany. [Online] 2009. http://jetcat.de/jetcatturbinen/strahlturbinen.htm.*

4. ***Roskam, Jan.*** *Airplane Flight Dynamics and Automatic Flight Controls. Lawrence, Kansas 66044 : DARcorporation, 1995. ISBN 1-884885-18-7.*

5. ***Unmanned Dynamics, LLC.*** *Aerosim Blockset, Version 1.2 User Guid. Hood River : Unmanned Dynamics, 2004.*

6. Federal Aviation Regulations. FAA Website. [Online] Federal Aviation Administration, 2007. http://www.airweb.faa.gov/Regulatory_and_Guidance_Library/rgFAR.nsf/MainFrame?OpenFrameSet.

7. ***Blair, Maxwell, et al.*** *A Joined-Wing Flight Experiment. Dayton : ARFL, 2008. ARFL-RB-WP-TR-2008-3101.*

8. ***Micropilot.*** *trueHWILmp. Micropilot.com. [Online] Micropilot, 2009. http://www.micropilot.com/products-truehwilmp.htm.*

9. ***Roskam, J.*** *Aircraft Design. Kansas : DARcorporation, 2004. ISBN 1-884885-43-8.*

10